Fire spread across pine needle fuel beds: characterization of temperature and velocity distributions within the fire plume

Fire Spread in Wildland Fuels: Characterization of Temperature and Velocity Distributions within the Fire Plume

Thierry MARCELLI, Paul-Antoine SANTONI, Albert SIMEONI, Eric LEONI

SPE – CNRS UMR 6134, ERT FEUX, Université de Corse, Campus Grossetti, B.P. 52

20250 Corte, France

and

Bernard PORTERIE

IUSTI – CNRS UMR 6595, ERT FEUX, Technopôle de Château-Gombert

5, Rue Enrico Fermi, 13453 Marseille Cedex 13, France

ABSTRACT

The aim of this article is twofold. First, it concerns the improvement of knowledge on the fundamental physical mechanisms that control the propagation of forest fires. To proceed, an experimental apparatus was designed to study, in laboratory conditions, the flame of a fire spreading across a pine needle fuel bed. Characterization of temperature was managed by using a reconstruction method based on a double thermocouple probe technique developed recently. The vertical gas velocity distribution was derived from the previous reconstructed signals by measuring the transit time of a thermal fluctuation between two points of the flow. Secondly, the experimental data were used for the testing of a physical two-phase model of forest fire behavior in which the decomposition of solid fuel constituting a forest fuel bed as well as the multiple interactions with the gas phase are represented.

NOMENCLATURE

C_{xy}	correlation function between signal x and y
C_p	specific heat at constant pressure
d	diameter of hot junction of a thermocouple
f_{vs}	volume fraction of soot
h	heat transfer coefficient
$\dot{m}$	masse rate
N	sample of size N
q	heat flux
Q	energy influx
r	distance between two probes
s^2	variance
t	time
T	temperature

Greek Symbols

α	Volume fraction
β	parameter defined in Eq. (15)
γ	gain coefficient
δ	parameter defined in Eq. (13)
ε	emissivity
η	linearization parameter
ξ	linearization function
θ	time shift
ρ	density
ρ_{xy}	correlation coefficient between signal x and y
σ	Stefan-Boltzmann constant
τ	time constant
Δt	time interval

Subscripts and superscripts

1, 2	thermocouple 1, 2
ash	ash
char	char
conv	convection
g	gas
H_2O	moisture
i	sample *i*
k	solid phase

pyr	pyrolizate gases
rad,abs	absorbed by radiation
$rad,lost$	lost by radiation
th	thermocouple
x	signal $x(t)$
y	signal $y(t)$

Diacritical

$\bar{}$	time average

1. INTRODUCTION

There is an abundant literature dealing with the modelling of fire spread in wildland fuels. Weber (1990) has classified mathematical fire spread models as statistical, empirical and physical models according to whether they involve no physics at all, no distinction between different modes of heat transfer (conduction, convection and radiation), or account each mechanism of heat transfer individually. The purpose of these models is mainly restricted to the prediction of the rate of the propagation. Since the pioneering work of Grishin (1978), physical models are becoming more and more complete as illustrated by the works of Grishin and co-workers (see the monograph of Grishin, 1997), Larini *et al.* (1998), Bellemare *et al.* (2001), Séro-Guillaume and Margerit (2002), to name but a few. They represent the most complete approach developed so far.

Physical models are generally based on a two-phase description of the medium: a gas phase flows through a bed which is viewed as an agglomeration of organic, randomly-oriented fuel elements. The bed is considered to be homogeneous, which means that all fuel elements have the same geometrical and thermo-physical properties, and therefore belong to the same class

of the solid phase. The gas and solid phase (the vegetation elements) in thermal non-equilibrium are assumed to be inter-dispersed and coupled by appropriate interaction terms. Each phase is treated as a continuum and is governed individually by a set of time-dependent equations. Then, any small volume in the domain of interest can be imagined as containing a volume fraction of each phase. The mathematical description of the physical problem is given below for a medium composed of a gas phase and a single-class solid phase. The generalisation to a multi-class solid phase can easily be obtained.

The physical two-phase model used in the present study may be considered as an extension of the formulation proposed by Grishin (1997). It describes the hydrodynamics through the fuel matrix and above the fuel bed, and incorporates first-order kinetics to describe drying, pyrolysis and combustion. Refined models for turbulence, turbulent combustion, radiation, and soot formation have been incorporated. This approach was tested against experiments with fires spreading across pine needles on the laboratory-scale. However, the only measurements available for comparison were coarse observations of the visible flame length or rate of spread (Porterie *et al.* 2000). Finest experimental measurements like gas temperature or velocity were not considered. It is particularly difficult to achieve reliable and accurate measurements of fluctuating temperatures for a fire spreading across pine needles. This lack of measurements of the turbulence of flames in wildland fuels is partly addressed in this paper to test the two-phase approach.

It should be recorded that the flames encountered in free burning forest fires are typical diffusion flames in which one can distinguish three behavioural regions. The lower part of the fire plume is the continuous flame region close to the source of the fire. Over that region, there is the intermittent one where balls of flame come away from the source, and the upper part is the conventional thermal plume. In this present study, only the lower and intermittent regions were investigated.

The aim of this work is twofold:

- Gas temperature and velocity measurements in a flame spreading across a fuel bed are provided. A reliable and robust experimental procedure was developed in a previous work (Santoni *et al.*, 2002) using a double thermocouple probe for reconstructing the fluctuations in gas temperature. This method is applied in this paper to measure the temperature distribution within the spreading fire plume. Then gas velocity measurements are provided from the method developed by Cox (1977), which considers the cross-correlation of random thermal fluctuations. The reconstruction for the gas temperature will appear as an important and innovative operation to perform before to determine the gas velocity using the cross-correlation technique.

- The multiphase model predictions of gas temperature and velocity for a fire spreading across a fuel bed are compared to the experimental measurements described here above. It should be noted that this model is tested against gas temperature and velocity measurements for the first time here.

2. MEASUREMENT METHODS FOR FLUCTUATING TEMPERATURE AND MEAN VELOCITY IN A FIRE PLUME

In this section, we present the methods used to measure the temperature and upward gas velocity. The first method consists in compensating thermocouple temperature by using a double thermocouple-probe technique for probe immersed in a flame, in order to restore the dynamic of the signals. Solely the major points of the compensation method are presented. The reader can refer to Santoni *et al.* (2002) for more details. The second one uses the statistical properties of the signals. A transit time of thermal fluctuation between two successive probes is extracted to measure the mean gas velocity (Cox, 1977).

2.1 Temperature Measurement

The measurement of the temperature is realised with exposed junction thermocouples, which have wires with different diameters. A model for the behaviour of the temperature of the thermocouple bead immersed in a flame was elaborated. This model was used to reconstruct the gas temperature

2.1.1 Linearized model of the thermocouple's bead temperature

The instantaneous heat balance for the bead of a thermocouple immersed in a continuous flame region was written thanks to the following hypotheses (Santoni *et al.*, 2002):

- the bead is supposed to be spherical and homogeneous,
- catalytic heat transfers are assumed negligible,
- conduction losses along the wires are not considered,
- convective heat flux is modeled by using Newton's law. We assume that this flux is homogeneous at the surface of the bead and given by

$$q_{conv} = -h\left(T_{th} - T_g\right), \qquad (1)$$

- if we further assume that the bead behaves like a gray body, the heat flux lost by radiation is given by

$$q_{rad,lost} = -\varepsilon_{th}\,\sigma\,T_{th}^4, \qquad (2)$$

- the last term to evaluate concerns the heat flux absorbed in the bead by radiation incoming from the surrounding flame. By assuming that the region of the flame surrounding the bead behaves like an isothermal homogeneous semi-transparent medium the following expression was derived

$$q_{rad,abs} = \varepsilon_{th}\,\sigma\,\varepsilon_g\,T_g^4. \qquad (3)$$

Finally, the instantaneous heat balance is

$$\frac{dT_{th}}{dt} = -\frac{6h}{\rho_{th} C_{p_{th}} d_{th}}\left(T_{th} - T_g\right) - \frac{6\varepsilon_{th}(1-\varepsilon_g)\sigma T_g^3}{\rho_{th} C_{p_{th}} d_{th}} T_g - \frac{6\varepsilon_{th}\sigma}{\rho_{th} C_{p_{th}} d_{th}}\left(T_{th}^4 - T_g^4\right) \qquad (4)$$

where d_{th} is the bead's diameter. Let assume that a parameter η can be defined so that

$$\left|\frac{T_g - \eta T_{th}}{T_g}\right| << 1 \qquad (5)$$

which means that $T_{th} \approx T_g / \eta$, we have

$$T_{th}^4 - T_g^4 \approx \xi(\eta) T_g^3 (T_{th} - T_g)$$

with $\xi(\eta) = 1 + \frac{1}{\eta} + \frac{1}{\eta^2} + \frac{1}{\eta^3}$. In the following, the parameter η will be omitted for simplicity and ξ will be written instead of $\xi(\eta)$. The heat balance for the thermocouple becomes

$$\tau(\xi)\frac{dT_{th}}{dt} + T_{th} = \gamma(\xi) T_g \qquad (6)$$

with

$$\tau(\xi) = \frac{\rho_{th} C_{p_{th}} d_{th}}{6(h + \xi\varepsilon_{th}\sigma T_g^3)}, \qquad (7)$$

and

$$\gamma(\xi) = \frac{h + \varepsilon_{th}(\xi - 1 + \varepsilon_g)\sigma T_g^3}{h + \xi\varepsilon_{th}\sigma T_g^3}. \qquad (8)$$

Large fluctuations of temperature, velocity and gas composition occur because of intermittency in buoyant flame. Hence the three unknowns h, ε_g and η fluctuate, and consequently also τ and γ. Instead of identifying h, ε_g and η, a method was elaborated to determine the two fluctuating parameters τ and γ. The use of mean parameters (for τ and γ) results in a somewhat inaccurate temperature measurement in turbulent combustion as demonstrated before (Vachon *et al.*, 1986; Tagawa and Ohta, 1997) for τ.

2.1.2 Parameter's identification

We consider two thermocouples, different only in diameter, that are immersed in the continuous region of a flame. They are set at a distance which ensures firstly that the velocity and temperature fields of the flow surrounding them are identical and secondly that there is no mutual perturbation of their boundary layers (Santoni *et al*., 2002). These conditions are necessary for the sensors to measure the same temperature T_g. If T_{th1} and T_{th2} denote the temperatures of the thin and thick thermocouples, respectively, their governing equations are

$$\begin{cases} \tau_1 \dfrac{dT_{th1}}{dt} + T_{th1} = \gamma_1 T_{g1} \\ \tau_2 \dfrac{dT_{th2}}{dt} + T_{th2} = \gamma_2 T_{g2} \end{cases} \quad (9)$$

The identification of the parameters is splitting up in two parts: the first one is devoted to the time constants identification, and the second one deals with the gain coefficients identification.

Time constant identification

To identify the time constants τ_1 and τ_2 the variance

$$s^2 = \frac{1}{N}\sum_{i=1}^{N}\left(\left(\gamma_2 T_{g2}^{\ i} - \gamma_1 T_{g1}^{\ i}\right) - \frac{1}{N}\sum_{i=1}^{N}\left(\gamma_2 T_{g2}^{\ i} - \gamma_1 T_{g1}^{\ i}\right)\right)^2 \quad (10)$$

was minimized for a number of N samples recorded by the thermocouples during a time interval Δt as follow:

$$\begin{cases} \dfrac{\partial s^2}{\partial \overline{\tau}_1} = 0 \\ \dfrac{\partial s^2}{\partial \overline{\tau}_2} = 0 \end{cases} \quad (11)$$

Since during Δt, τ_1 and τ_2 are assumed constant, we note them from now on $\overline{\tau_1}$ and $\overline{\tau_2}$.

Gain coefficient identification

As previously for the time constants identification, two more relations are needed to identify the gain coefficients. The averaged gain coefficients $\overline{\gamma_1}$ and $\overline{\gamma_2}$ are considered below since they depend on $\overline{\tau_1}$ and $\overline{\tau_2}$. Considering Eqs. 7 and 8, a first relation between the gain coefficients was derived

$$\overline{\gamma_1} - \delta\overline{\gamma_2} = 1 - \delta \qquad (12)$$

with

$$\delta \approx \frac{\overline{\tau_1}}{\overline{\tau_2}} \frac{d_{th2}}{d_{th1}}. \qquad (13)$$

The second relation is derived by assuming that the two thermocouples are close enough to allow $T_{g1} \approx T_{g2}$. We obtain from Eqs 9:

$$\overline{\gamma_1} - \beta\overline{\gamma_2} = 0 \qquad (14)$$

with

$$\beta = \frac{\frac{1}{N}\sum_{i=1}^{N}\left(\overline{\tau_1}\frac{dT_{th1}^{i}}{dt} + T_{th1}^{i}\right)}{\frac{1}{N}\sum_{i=1}^{N}\left(\overline{\tau_2}\frac{dT_{th2}^{i}}{dt} + T_{th2}^{i}\right)} \qquad (15)$$

Thus by solving the set of Eqs 12 and 14, we can evaluate $\overline{\gamma_1}$ and $\overline{\gamma_2}$. Finally, the gas temperature is reconstructed from Eqs 9.

2.2 Velocity Measurement

The principle of the method to calculate the vertical gas velocities is based on the measure of the transit time of a thermal fluctuation between two points of the flow (Cox, 1977). For this, we use the correlation concept where the degree of association of certain variables is to be measured. The statistical properties of the signals are employed to recognise a fluid fluctuation pattern and to time its movement. It is assumed that this pattern changes little for a

small separation r between two probes. The transit time θ_0 is that value of time shift for which the delayed version $x(t-\theta)$ of signal $x(t)$ from the first measuring point is almost equal to the signal $y(t)$ from the second point, *i.e.* when the cross-correlation function

$$C_{xy}(r,\theta) = \lim_{\chi\to\infty} \frac{1}{\chi} \int_0^{\chi} x(t-\theta)\, y(t)\, \mathrm{dt} \qquad (16)$$

has a maximum value. This function is often expressed in normalised form as the correlation coefficient $\rho_{xy}(r,\theta)$ where

$$\rho_{xy}(r,\theta) = \frac{C_{xy}(r,\theta)}{\left[\overline{x(t-\theta)^2}\right]^{\frac{1}{2}} \left[\overline{y(t)^2}\right]^{\frac{1}{2}}} \qquad (17)$$

with $\overline{x(t-\theta)^2} = \lim_{\chi\to\infty} \frac{1}{\chi} \int_0^{\chi} x(t-\theta)^2 dt$.

When $r=0$, $y(t)=x(t)$ then the cross-correlation function becomes the auto-correlation function of *x(t)*

$$C_{xx}(0,\theta) = \lim_{\chi\to\infty} \frac{1}{\chi} \int_0^{\chi} x(t-\theta)\, x(t)\, \mathrm{dt}\,. \qquad (18)$$

The auto-correlation function describes the relationship between a signal and its time-shifted versions, and serves as an indicator of the validity of Taylor's assumption of frozen turbulence (Cox, 1977), which states that fluctuations are frozen into the mean flow. It means that the cross-correlation function is identical to the auto-correlation function with a time-shift θ_0: $C_{xy}(r,0) = C_{xx}(0,\theta_0)$. However, actually, it is not the case due to viscous dissipation of the eddies. The cross-correlation coefficient is poorer than the auto-correlation one. A measure of the departure from this assumption will be considered in the paper by a comparison of the space correlation, $C_{xy}(r,0)$, the relation between the instantaneous signals at two separated points, with the auto-correlation, $C_{xx}(0,\theta_0)$.

3. THE PHYSICAL MODEL

3.1 Model overview

In the present physical model, the gas phase is computed by solving the two-phase, Favre density-weighted averaged Navier-Stokes equations, in connection with the RNG (Renormalization Group theory) k-ε turbulence model with additional buoyancy-driven production/destruction (Yakhot and Orzag, 1986).

The gas phase equations and the constants of the turbulence model are given in the Appendix. A detailed presentation of these equations has been done elsewhere (Porterie et al., 2000; Bellemare et al., 2001) and is not repeated here. The ideal-gas law is used to calculate density variations, and the specific heat and viscosity for each species of the gas phase are a function of temperature and composition. Radiative exchanges between hot combustion products and the virgin combustible fuel bed are a critical aspect of flame propagation and the incandescent soot particles are main contributors to the overhead flame radiation. The chemical nature of the burning material and local specific fire conditions can lead to a large production of soot. An accurate prediction of the radiative transfer requires accounting for soot production/destruction, especially in turbulent flames. The soot model is identical to the one proposed by Kennedy et al. (1990) for ethylene/air diffusion flames. Only one equation is used, namely the transport equation for the volume fraction of soot, f_{vs}.

Concerning the solid phase, the following assumptions are used: i) the position of individual fuel elements are assumed to be fixed in space; ii) Particles are assumed to be isothermal (thermally thin assumption). Allowing for these assumptions, the governing equations reduce to the following ordinary differential equations for describing the temporal changes of the particles with respect to mass and temperature:

$$\frac{\partial(\alpha_k \rho_k)}{\partial t} = -\dot{m}_k = \dot{m}_{k,H_2O} + \dot{m}_{k,char} + \dot{m}_{k,pyr} + \dot{m}_{k,ash} \qquad (19)$$

$$\alpha_k \rho_k C_{pk} \frac{\partial T_k}{\partial t} = Q_{k,chemical} + Q_{k,radiative} + Q_{k,convective} \quad (20)$$

It is worth noting that the rate of particle mass reduction relative to the thermal decomposition of the solid phase can be represented by the sum of the mass rates due to water vaporization, pyrolysis, char combustion, and ash formation. In the energy equation, the three right-hand-side terms correspond to the chemical energy influx due to the thermal degradation of the solid phase, the radiative energy influx at the surface of the solid phase, and the convective energy influx, respectively.

The chemical reaction, soot formation, and radiation sub-models used in the physical model along with the constitutive relations for drag and convective heat transfer between the two phases are not detailed here for clarity, but the interested reader can refer to Porterie *et al*. (2000).

3.2 Numerical procedure

The governing equations for the gas phase are discretized on a non-uniform grid using a finite-volume procedure along with a second-order backward Euler scheme for time integration. Diffusion terms are approximated using a second-order central difference scheme whilst convective ones are discretized using a high-order upwind scheme, namely the ULTRASHARP approach (Leonard and Mokhtari, 1990; Leonard, 1991; Leonard and Drummond, 1995). This combines the use of a high-order upwind scheme for the convective terms and a flux limiter strategy to eliminate any possibility of overshoot, undershoot or oscillation sometimes introduced by the convective schemes when the monotonicity of the solution is not ensured.

Since the transient behavior is of interest, the pressure-velocity linked equations are solved using the Iterative PISO algorithm (Pressure-Implicit with Splitting of Operators) developed

by Chow and Cheung (1997). The ordinary differential equations governing the behavior of the solid phase are solved using a fourth-order Runge-Kutta scheme.

The resulting systems of linear algebraic equations for each variable are then solved iteratively using the line-by-line tridiagonal matrix algorithm (TDMA) (Patankar, 1980). In order to accelerate convergence and prevent low-frequency behavior of the solution typical of this type of buoyancy-driven flow, all the gas variables are under-relaxed using inertial relaxation (Patankar, 1980).

All the computations have been carried out using a Cartesian non-uniform grid covering a space domain of 5 $m \times 4$ m and comprising 325×90 cells in the x and y directions with 285 constant size cells from x =2 m to x = 2.85 m, and 10 constant size cells over the height of the fuel bed. Finer grids were tested to ensure that the numerical results were grid-independent. The time step is 0.01 s. The CPU time on a 2.2 GHz workstation is about 10 h.

4. EXPERIMENTAL PROCEDURES

Experimental fires were conducted at the University of Corsica laboratory in a closed room without any air motion. Smoke was removed from the room after each test. The properties of the ambient air were measured for each test; the temperature ranged between 25 to 30°C and the relative humidity varied from 40 to 50%.

4.1 Experimental device

Figure 1 shows the set-up, including two trees of 4 thermocouple-probes. Each probe is composed of a two-hole insulator made of recrystallized pure alumina ceramic containing over 99.8% Al_2O_3. The insulators were 28.5 cm long (o.d. 3.1 mm; i.d. 1 mm). The thermocouples were threaded through these holes and their junctions were set at a distance of about 0.3 mm from each other. The ratio between the diameters of the thermocouples' beads is

about 2 for all probes. Those insulators protected the thermocouples' stainless steel sheaths. The flame could warm their sheath without this protection and may well altered the measurements. The thermocouples' beads were cleaned after each run. Thermocouple-probes are placed in the following way: the first probe takes place on the top of the litter, the second one is at 2 *cm* from the first one, as well as the third one from the second one and the others are placed 4 *cm* apart (see Table 1). The mount effects on the hydrodynamic and hence on the recorded temperature were assumed negligible.

The experimental apparatus was composed of a syporex plate (1.2 *m* long and 0.5 *m* wide) protected by sand (Figure 1). Pure oven-dried pine needles were spread as evenly as possible on a portion (0.7 *m* long and 0.4 *m* width) of the total area of the combustion table to give a homogeneous structure, representative of a typical layer found in Corsican forests with a load of approximately 0.5 $kg.m^{-2}$ on a dry basis. The syporex plate was further supported by a larger table (1.5 *m* long and 1 *m* wide) to allow lateral inflows of air. Three experiments were performed to observe the spread of the fire under no slope and without any wind for line-ignition fires. For these, a line was ignited using alcohol at one small edge of the fuel-bed, as shown in Figure 1. The arrays of double thermocouple probes were installed above the fuel at approximately 0.35 *m* before its end, *i.e.* far enough from the ignition line for a fire to achieve a stable spread-rate and flame shape, before it passed through the thermocouples. The constant spread-rate was confirmed by using the temperatures recorded by five double thermocouple-probes located on the top of the litter and spaced 0.1 *m* apart along its main axis. Those probes are not shown on Figure 1 for more legibility.

4.2 Fuel bed

The fuel bed was composed of *Pinus pinaster* dead needles. Their area to volume ratio and density are 4550 m^{-1} and 680 $kg.m^{-3}$, respectively. The depth of fuel was approximately

2.3 cm, giving a bulk density of 21.74 $kg.m^{-3}$ and a packing ratio of 0.032. The needles were dried in an oven at 60°C for 24 hours before each experimental run. Since they partially re-hydrated during their removal from the oven and the ignition, a sample of needles was loaded to evaluate the fuel moisture content before each run. It was found that the needles were conditioned to a moisture content of 1% - 3%.

4.3 Instruments

The thermocouples used in these experiments were mineral-insulated integrally metal-sheathed (MIMS) pre-welded type K (chromel-alumel) pairs of wire with an exposed junction. The MIMS form of thermocouple consisted of matched thermocouple wires surrounded by insulating material compacted by rolling until the sheath is reduced in diameter. In this work, we used cheap stainless steel sheathed (304 SS) and M_gO insulated standard thermocouples (Omega Engineering). The exposed junction consists of an extended going junction beyond the protective metallic sheath to give accurate fast response. The double thermocouple probe consisted of two 30 cm long sensors with sheaths of 250 and 500 μm in diameter for both thin and thick thermocouples. At the exposed hot junctions the wires were 50 and 100 μm in diameter, respectively. The exposed junctions were nearly perfect spheres, whose diameters varied from 100 to 225 μm and from 250 to 425 μm, respectively. The wire diameters were chosen since they constituted a compromise between their robustness and their rapidity (low time constant). Furthermore, the size of the wires adopted here limit the sagging of the junction due to thermocouple expanding. This prevented us from using other supports (Mcenally *et al.*, 1997), which are inappropriate in our case. The thermocouples were connected to a Hewlett Packard (HP E9811B) data logger, which is a programmable unit. It possesses an on board digital signal processor, which converts the voltage read across the analog input channel and applies a high speed conversion, which

produces measurements of temperature. The sampling frequency was 700 *Hz*; the precision in temperature measurement was 0.5°*C*.

5. RESULTS AND DISCUSSION

5.1 Temperature

Figure 2 shows the temperature curves versus time of two thin thermocouples. The first one (thermocouple number 1) takes place at 4 *cm* from the ground (top of the litter) and the second one (number 6) at 20 *cm* (see Table 1). A qualitative description of the burning processes with reference to the temperature curve of thermocouple number 1 is first provided to detail the spreading features. The thermocouple curve reveals a temperature increase as the fire approaches until it reaches the thermocouple. Heat is transferred from the hot flame to the unburned fuel bed, the temperature of which increases. When this fuel becomes hot enough, it vaporizes. The resulting gaseous fuel reacts once it has come into contact with oxygen and a flame ensues. The signal fluctuates around some sort of average value, meaning that the sensor is immersed in the flame. After this zone, which lasts several seconds (depending on fuel conditions), the flame decreases in size and hence temperature due to a lack of readily available fuel.

Figure 2 shows two kinds of temperature growth. The lower thermocouple (number 1), which takes place on the top of the litter, is firstly heated in a more regular and less fluctuating way than the upper one. We can notice that a few seconds before the ignition of the litter, the temperature of the thermocouple (number 6) increases more significantly. This points out the growth of the fire plume radius with height, which heats the upper thermocouple before the lower one. Then, when the litter ignites the two thermocouples are immersed in the flame. During this stage, the temperature profiles show two properties of the gas flow. The temperature fluctuates less on the top of the litter than above it. This reveals the laminar

feature of the flow in the ejection zone of the pyrolyzate gases, before it becomes turbulent with height.

Figure 3 displays the temperature curves of a double thermocouple probe before and after the numerical compensation. The reconstruction for the gas temperature provided here was performed for a thermocouple (number 6) located in the fully developed flame zone. Solely a portion of the reconstructed temperature is displayed, which corresponds to the time interval when the temperature fluctuates around the maximum temperature. In this time interval, the reconstructed temperature curves have a correlation coefficient of more than 99%. Afterwards, the compensation was applied for the whole set of double thermocouple probes. Since the multiphase fire spread model provides mean time averaged quantities, the compensated temperatures were averaged for comparison with the model predictions. The averages were calculated on the time interval associated with the zone of maximum temperature, which corresponds to the flame resident time. This was performed on both compensated and thin thermocouples temperatures to examine the effect of the compensation. Figure 4 shows the mean profiles versus height of these two temperatures. We can observe that the numerical compensation modifies a little bit the averaged values of the thin thermocouples, while keeping the shape of the temperature profiles. The interest of the compensation technique relies more on the render of the dynamic of the signals (as shown in Figure 3) than in the correction of its mean value. This advantage will be put to the fore in the next section. Figure 5 displays the set of compensated temperature profiles for the different experiments. Like McCaffrey (1979), Cox (1985) and Dupuy (1998), we can observe two behaviours. The first one concerns the temperature increase just above the litter. In this region there is an oxygen default due to the ejection of the pyrolyzate gases, so combustion is incomplete. Then the pyrolyzate gases burn when they reach the oxygen and the mean temperature is maximum (here about 1050°C). The second behavioural zone corresponds to

the typical cooling of the fire plume. The temperature deviations observed for the experiments are certainly due to the heterogeneity of the fuel bed, even if the needles were spread as evenly as possible on the combustion bench.

Figure 6 shows the time evolution of gas temperature contours predicted by the two-phases model, from $t = 90\ s$ to $102\ s$ every 4 seconds, as the fire plume is going by the thermocouple tree. Buoyancy effects lead to small-amplitude oscillations of the fire plume as usually observed in natural fires. These temperature fluctuations are smaller in the lower part of the fire plume, as seen from experiments (Figure 2). Although the code is used in its time-dependent mode, a genuine steady-sate solution is obtained with a steady rate of fire spread (ROS) of 0.32 *cm/s*. Our model slightly overestimates the experimental mean rate of spread which is of 0.29 *cm/s*. This result seems to be due to a slight overestimation of radiation which is the mechanism which controls the preheating process of the combustible bed for no-wind conditions (It must be kept in mind that fuel elements can receive radiation coming from the overhead flame and from other particles). Every second from $t = 96\ s$ to $99\ s$, computed gas temperature profiles are compared to the experimental profiles determined from 3 replications (Figure 7). The same general behaviour is observed but the estimated high-temperature region is located slightly lower than experimentally observed. It is obvious that model predictions reveal an overestimation of the ROS as well as a downward shift of the high-temperature zone suggesting that the most intense combustion occurs in the lower part of the external flaming zone, too close to the top of the fuel bed. This phenomenon can explain partly the overestimation of radiation mentioned above.

5.2 Velocity

Figure 8 displays the auto-correlation function for a thin thermocouple temperature before and after the numerical compensation. We can notice that the reconstruction of the signal allows

to accentuate the peak (at $\theta = 0$). It restores the dynamic of the temperature signal lost by the thermocouple, which acts as a low-pass filter on the gas temperature. The method used to calculate the gas velocity is based on the transit time measurement of a thermal fluctuation between two parts of the flow (see section 2.2), and will be more efficient with the reconstructed signals. Conversely to Dupuy (1998), it is not necessary to apply a high-pass filter to the signal in order to carry out the main value to keep only the "high" frequencies to calculate the gas velocity.

To implement this method, it is necessary to verify the assumption of frozen turbulence, however. This assumption was investigated for two successive probes signals as mentioned in section 2.2. Figure 9 presents such compensated signals of temperature for two probes 4 *cm* apart on a short time interval. Each fluctuation of the compensated temperature of the lower probe is observed with a time shift on the compensated temperature of the upper one. Figure 10 shows that the assumption of frozen turbulence appears reasonable, for example, for probes 4 and 5 (located at 0.12 *cm* and 0.16 *cm* from the ground, respectively). The cross-correlation coefficient for these probes shows a peak, which appears at time shift $\theta_0 = 0.0364\ s$. We can see that the cross-correlation coefficient $\rho_{45}(0.04, 0) \approx 0.36$ is near to the auto-correlation coefficient with time shift θ_0 for probe number 4 $\rho_{44}(0, \theta_0) \approx 0.38$. The delayed correlation is poorer because of viscous dissipation of the eddies. The assumption of frozen turbulence was verified for each pair of successive probes before calculating the mean gas velocities along the fire plume.

Another feature, which is noticeable, concerns the increase of the cross-correlation coefficient peak with height. For probes located within the 4 *cm* above the top of the litter, the peak in the cross-correlation coefficient is slightly distinguishable in spite of the compensation on the temperature signals (Figure 11). The reason is the small degree of frequency variability present for the lower temperature signals. Indeed the flow is laminar in the near fire plume.

Upward gas velocities, determined by cross-correlation technique, versus height, are plotted in Figure 12. The velocities were calculated for each pair of successive probes in the same time interval as those previously mentioned for the calculation of the mean maximum temperature. We can note that the profiles follow the same tendency for the three experimental runs. In the lower part of the fire plume (height $< 0.1\ m$), the measured velocities are rather different. This is due to the laminar pattern of the flow as previously mentioned. The cross-correlation technique lies in the measure of the transit time of thermal fluctuation. Obviously, the velocity calculation is less efficient in the near fire plume than in the above regions since the temperature signals present less fluctuations. Conversely, in the upper part of the flow the measured velocities are very close at each probe interval for each experimental run. The absolute error on transit time determination is assumed equal to the sampling period ($0.0014\ s$) since the transit time is longer than this period. This leads to relative errors under 10% on the determination of the gas flow velocity (see table 2).

The mean gas velocities displayed in Figure 12 for the three experiments were averaged for comparison with the multiphase model predictions. Figure 13 indicates correct trends with a slight overestimation of the predictions in the flame region as well as temperature (Figure 7). The early thermal expansion of gases due to the heat created by the combustion leads to higher estimated convective accelerations than those determined from experiments.

6. CONCLUSION

The main contributions of this work can be summarized as follow:

- A simple, sound and cheap experimental set-up was built to investigate gas temperature and velocity in the fire plume during the spreading of a line-fire across a fuel bed. This set-up and the method developed to reconstruct the gas temperature by using double

thermocouple-probes have provided results useful for testing models of fire spread. In particular, the analytical method used to estimate the upward gas velocity from compensated thermocouple's signals led to relative errors on velocity under 10% for the different experiments. The coupling between these two methods is innovative and brings a valuable improvement on the estimation of the gas velocity in the flame (Dupuy, 1998).

- On the other hand, the comparisons between the experimental data and the multiphase model predictions are encouraging. The simulated and observed temperature and velocity profiles were very close. The model slightly overestimates the rate of spread. This result was attributed to an overestimation of radiation that controls mainly the preheating process of the fuel under no wind condition.

This work represents the first step for testing physical models with accurate experimental measures. Further studies are necessary to improve the multiphase model validation. Fuel load and fuel moisture content effects on the temperature and velocity distribution within the fire plume will be investigated in future work.

REFERENCES

Bellemare, L. O., Porterie, B. and Loraud J. C. (2001) On the prediction of firebreak efficiency. *Combust. Sci. Tech.*, **163**, pp. 131-176.

Chow, W. K., and Cheung Y. L. (1997) Comparison of the algorithms PISO and SIMPLER for solving pressure-velocity linked equations in simulating compartment fire. *Num. Heat Transfer*, Part A, **31**, pp. 87-112.

Cox, G. (1977) Gas Velocity Measurement in Fires by the Cross-Correlation of Random Thermal Fluctuations – A Comparison with Conventional Techniques. *Combust. and Flame*, **28**, pp. 155-163.

Cox, G. and Chitty, R. (1985) Some source-dependent effects of unbounded fires. *Combust. and Flame*, **60**, pp. 219-232.

Dupuy, J. L., Maréchal, J., Bouvier, L., and Loïs, N. (1998) Measurement of Temperatures and Radiant Fluxes during Static Fires in a Pourous Fuel. *III Int. Conf. on Forest Fire Res.*, Luso, Portugal, **1**, pp. 843-858.

Grishin A.M. (1978) Mathematical modelling of forest fires. *Num. Methods in Continuum Mechanics.* Novosibirsk, Institute of Theoretical and Applied Mechanics of the Siberian Branch of the Academy of Sciences of USSR, **9**, pp. 30-56.

Grishin, A. M. (1997) Mathematical Modeling of Forest Fires and New Methods of Fighting Them. *Publishing House of the Tomsk State University*, p. 91

Kennedy, I. M., Kollmann, W. And Chen J.-Y. (1990) A model for soot formation in a laminar diffusion flame. *Combust. and Flame*, **81**, pp. 73-85.

Larini, M., Giroux F., Porterie B., and Loraud J. C. (1998) A Multiphase Formulation for Fire Propagation in Heterogeneous Combustible Media. *Int. J. of Heat and Mass Transfer*, **41** (6-7), pp. 881-897.

Leonard B. P. and Mokhtari S. (1990) Beyond first-order upwinding: the ultrasharp alternative for non-oscillatory steady-state simulation of convection. *Int. J. Num. Methods Eng.*, **30**, pp. 729-766.

Leonard B. P. (1991) The ultimate conservative difference scheme applied to unsteady one-dimensional advection. *Comput. Methods Appl. Mech. Eng.*, **88**, pp. 17-74.

Leonard B. P. and Drummond J.E. (1995) Why you should not use hybrid, power-law or related exponential schemes for convective modelling. There are much better alternatives. *Int. J. Num. Methods Eng.*, **20**, pp. 421-442.

Mc Caffrey, B. J. (1979) Purely buoyant diffusion flame: Some experimental results, *NBSIR* 79-1910, National Bureau of Standard, Department of Commerce, Washington DC 20234.

Mcenally, C. S., Köylü, Ü. Ö., Pfefferle, L. D. and Rosner, D. E. (1997) Soot volume fraction and temperature measurements in laminar nonpremixed flames using thermocouples. *Combust. and Flame* **109**, pp. 701-720.

Patankar, S. V. (1980) Numerical Heat Transfer and Fluid Flow. *Hemisphere Publishing Corporation*, 198 pages.

Porterie, B., Morvan, D., Loraud, J. C. and Larini, M. (2000) Firespread through fuel beds: Modeling of wind-aided fires and induced hydrodynamics. *Phys. of Fluids*, **12**(7), pp. 1762-1781.

Santoni, P. A., Marcelli, T. and Leoni, E. (2002) Measurement of Fluctuating Temperatures in a Continuous Flame Spreading Across a Fuel Bed Using a Double Thermocouple Probe. *Combust. and flame* (To be published).

Sero-Guillaume, O. and Margerit, J. (2002) Modelling Forest fire: Part 1 and Part 2, *Int. J. Heat Mass Transfer*, **45**, pp. 1705-1737.

Tagawa, M., and Ohta, Y. (1997) Two-thermocouple probe for fluctuating temperature measurement in combustion – Rational estimation of mean and fluctuating time constants. *Combust. and Flame*, **109**, pp. 549-560.

Vachon, M., Cambray, P., Maciaszek, T., and Bellet, J.V. (1986) Temperature and velocity fluctuation measurements in a diffusion flame with large buoyancy effects. *Combust. Sci. Tech.*, **48**, pp. 223-240.

Weber, R.O. (1990) Modelling fire spread through fuel beds. *Prog. in Energy and Combust. Sci.*, **17**, pp. 67-82.

Yakhot, V. and Orzag, S. (1986) Renormalization group analysis of turbulence. *J. Sci. Comput.*, 1 (3), pp. 3-52.

APPENDIX: Model equations

The general form of the transport equations of the gas phase is the following:

$$\frac{\partial}{\partial t}(\rho\Phi)+\frac{\partial}{\partial x_j}(\rho u_j \Phi)=\frac{\partial}{\partial x_j}\left(\Gamma_\Phi \frac{\partial \Phi}{\partial x_j}\right)+S_\Phi \qquad (1)$$

where: Φ is any transported property (species mass fraction, momentum through two velocity components, turbulent kinetic energy, rate of dissipation of turbulent kinetic energy, soot volume fraction or energy by means of the enthalpy); Γ_Φ and S_Φ are the diffusion exchange coefficient and source/sink terms for Φ. They are summarized as follow

Transport of	Φ	Γ_Φ	S_Φ
Mass	1	0	0
Momentum	u_i	μ_{eff}	$-\alpha_g \frac{\partial p_g}{\partial x_i}+\rho g_i$ $+\frac{\partial}{\partial x_j}\left[\mu_{eff}\left(\frac{\partial u_i}{\partial x_j}+\frac{\partial u_j}{\partial x_i}\right)\right]$ $-\frac{\partial}{\partial x_j}\left[\frac{2}{3}\mu_{eff}\frac{\partial u_k}{\partial x_k}\delta_{ij}\right]-F_i$
Enthalpy	h	$\frac{\mu}{\mathrm{Pr}}+\frac{\mu_t}{\sigma_t}$	$-Q_{g,radiative}+Q_{k,convective}+S_h$
Kinetic energy of turbulence	k	$\mu+\frac{\mu_t}{\sigma_k}$	$P+W-\rho\varepsilon$
Rate of dissipation of k	ε	$\mu+\frac{\mu_t}{\sigma_\varepsilon}$	$(C_{\varepsilon 1}-R)\frac{\varepsilon}{k}P-C_{\varepsilon 2}\rho\frac{\varepsilon^2}{k}$ $+C_{\varepsilon 3}\frac{\varepsilon}{k}W$
Soot volume fraction	f_{vs}	$\frac{\mu_t}{\sigma_f}$	$-\frac{\partial}{\partial x_j}\left(0.55\mu\frac{1}{T}\frac{\partial T}{\partial x_j}f_{vs}\right)-\rho\frac{\nu_s \dot{m}_{pyr}}{\rho_s}$ $-\rho\frac{6.5 f_{vs} p_{O2}}{\rho_s d_s\sqrt{T}}\exp(-19750/T)$
Species mass fraction	Y_α	$\frac{\mu}{Sc}+\frac{\mu_t}{\sigma_f}$	$\dot{\omega}_\alpha+S_{Y_\alpha}$

where $\rho=\alpha_g\rho_g$, $\mu=\alpha_g\mu_g$, $\mu_t=\rho C_\mu\frac{k^2}{\varepsilon}$, $\mu_{eff}=\mu+\mu_t$.

The three source terms in the transport equation of soot account for the thermophoresis, formation, and oxidation processes, respectively, and ρ_s=1800kg/m^3 is the soot density. The terms F_i, S_h, $S_{Y\alpha}$, and $\dot{\omega}_\alpha$ are the drag force, the chemical sources of enthalpy and species as a consequence of thermal degradation of the fuel material, and the chemical source of species as a consequence of homogeneous reactions.

The shear and buoyancy turbulent production/destruction terms P and W can be expressed by

$$P = -\left[\mu_t\left(\frac{\partial u_i}{\partial x_j}+\frac{\partial u_j}{\partial x_i}\right)-\frac{2}{3}\left(\mu_t\frac{\partial u_k}{\partial x_k}\delta_{ij}+\rho k\right)\right]\frac{\partial u_i}{\partial x_j},\ W = -\beta g\frac{\mu_t}{\sigma_t}\frac{\partial T}{\partial x_j}$$

With

$$R = \frac{\eta\left(1-\eta/\eta_0\right)}{1+\beta\eta^3} \qquad \eta = \sqrt{\left|\frac{P_k}{\rho C_\mu \varepsilon}\right|} \quad \eta_0 = 4.38 \quad \beta = 0.015 \quad C_\mu = 0.0845$$

$$\sigma_k = 0.7179 \quad \sigma_\varepsilon = 0.7179 \quad \sigma_f = \sigma_t = 0.7 \quad Sc = \Pr = 0.71$$

$$C_{\varepsilon 1} = 1.42 \qquad C_{\varepsilon 2} = 1.68 \qquad C_{\varepsilon 3} = 1.5$$

Equations of state

The gas is assumed to be a mixture of perfect gases and including the chemical energy in the mixture static enthalpy, the equations of state will take the form

$$p_g = \rho_g RT\sum_\alpha \frac{Y_\alpha}{W_\alpha} \tag{2}$$

$$h = \sum_\alpha Y_\alpha\left(\Delta h^0_{f\alpha} + \int_{T_0}^{T} C_{p\alpha}(T)\,dT\right) \tag{3}$$

Table 1: Double thermocouple-probes positions

Probe	1	2	3	4	5	6	7	8
Height (m)	0.04	0.06	0.08	0.12	0.16	0.20	0.24	0.28

Table 2: Transit times and mean upward gas velocities for three experiments

Probe interval (m)	Transit time (s)			Velocity ($m.s^{-1}$)			Averaged relative error (%) on estimated velocity
	Exp 1	Exp 2	Exp 3	Exp 1	Exp 2	Exp 3	
0.04 – 0.06	0.0378	0.0518	5.5555	0.5291	0.3861	0.0036	2.04 %
0.06 – 0.08	0.0196	0.0238	0.0308	0.7519	0.8403	0.6494	7.85 %
0.08 – 0.12	0.0420	0.0476	0.0406	0.9524	0.8403	0.9852	3.28 %
0.12 – 0.16	0.0364	0.0336	0.0336	1.0989	1.1905	1.1905	4.40 %
0.16 – 0.20	0.0294	0.0322	0.0294	1.3605	1.2422	1.3605	6.80 %
0.20 – 0.24	0.0308	0.0308	0.0278	1.2987	1.2987	1.4286	6.18 %
0.24 – 0.28	0.0252	0.0266	0.0266	1.5873	1.5038	1.5038	9.34 %

LIST OF FIGURES

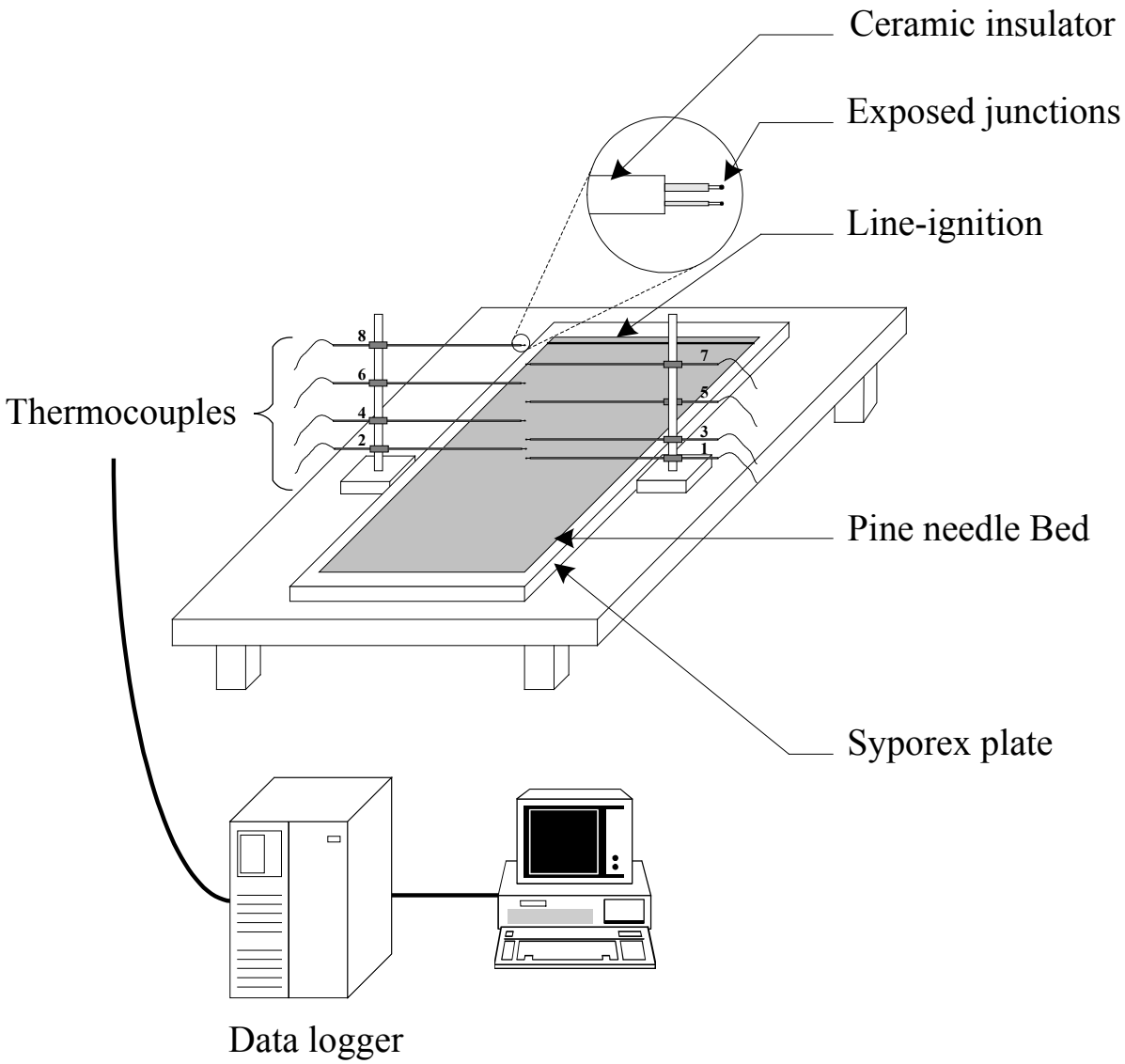

Figure 1: Experimental set-up to study fire plume

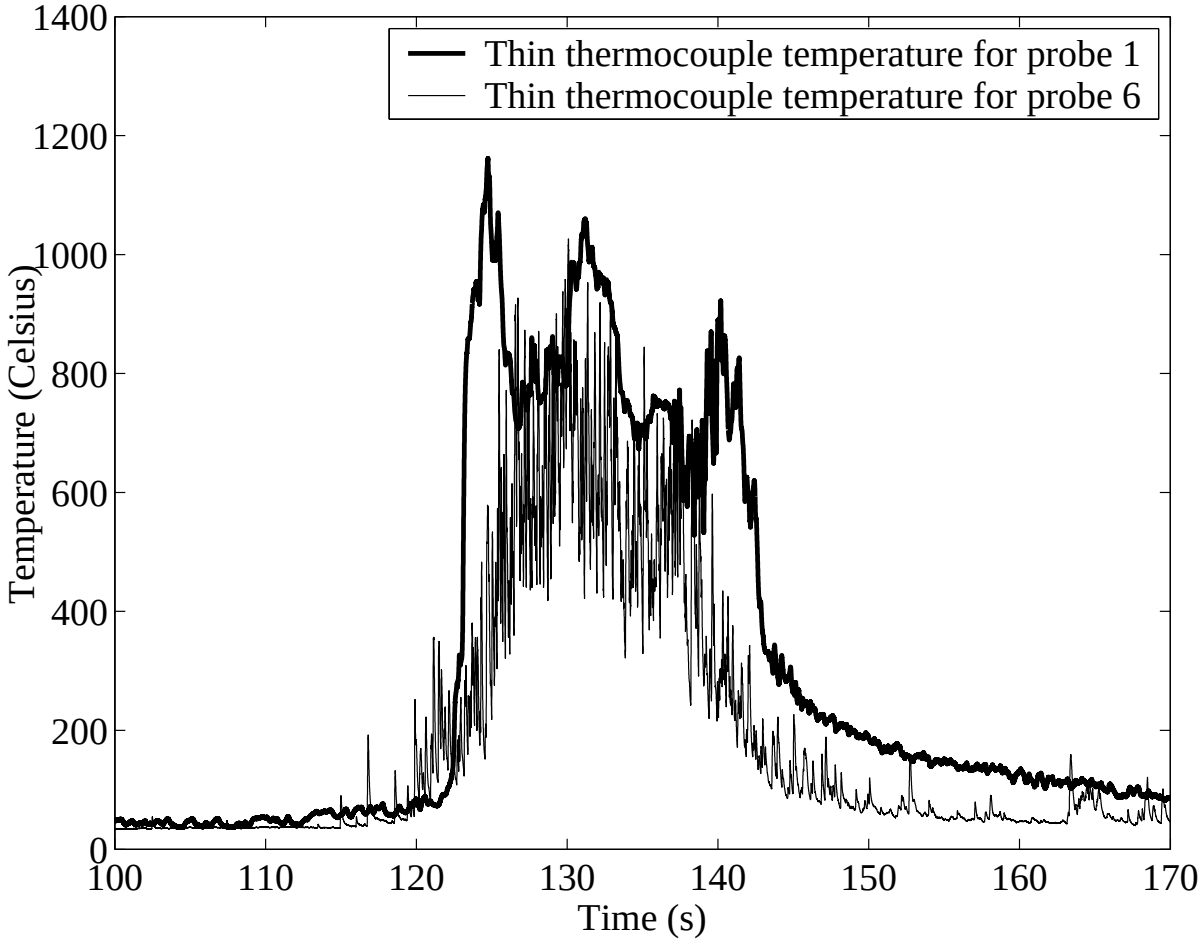

Figure 2: Temperatures of two thin thermocouples located at two different heights

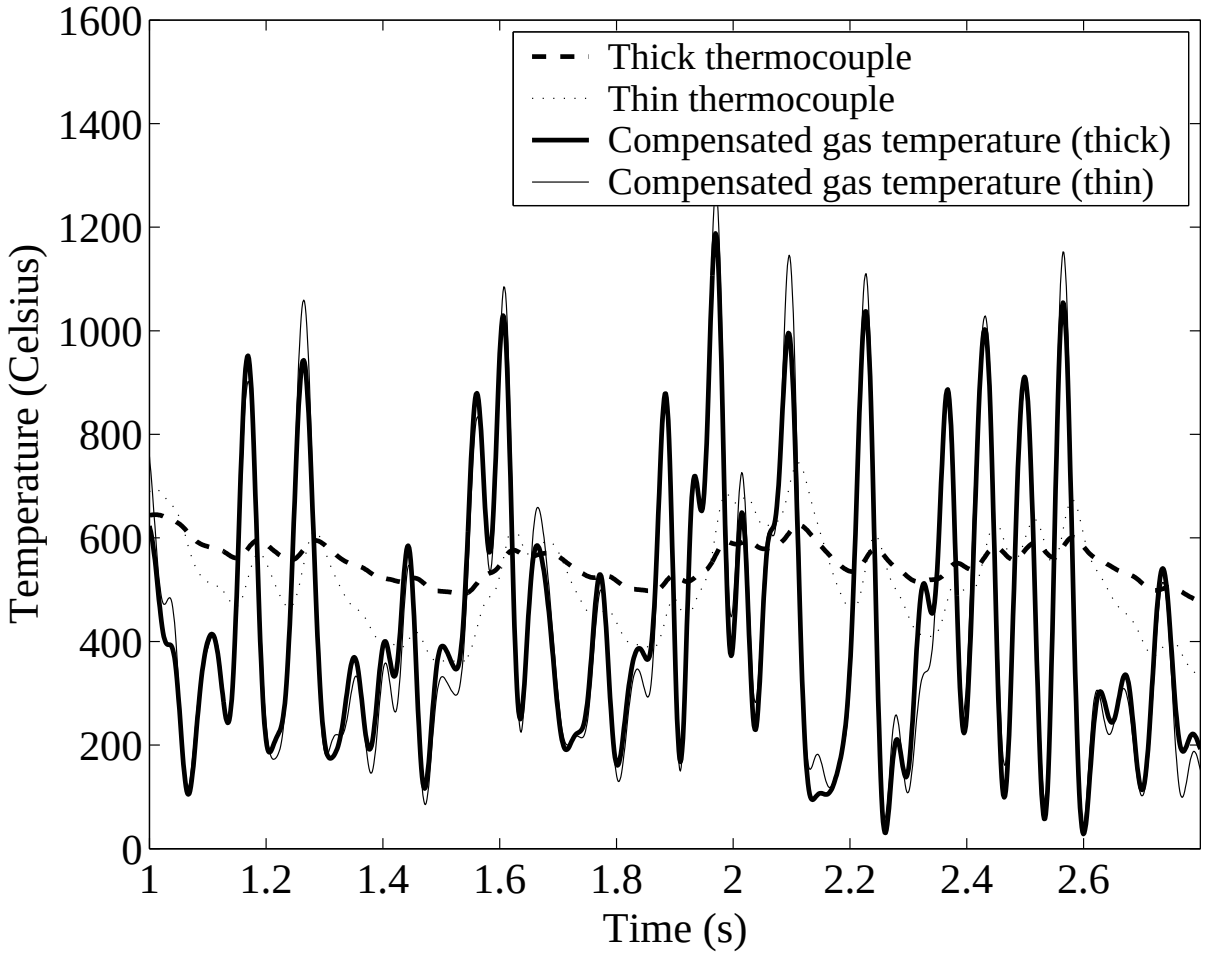

Figure 3: Example of numerical compensation for the gas temperature (probe 5).

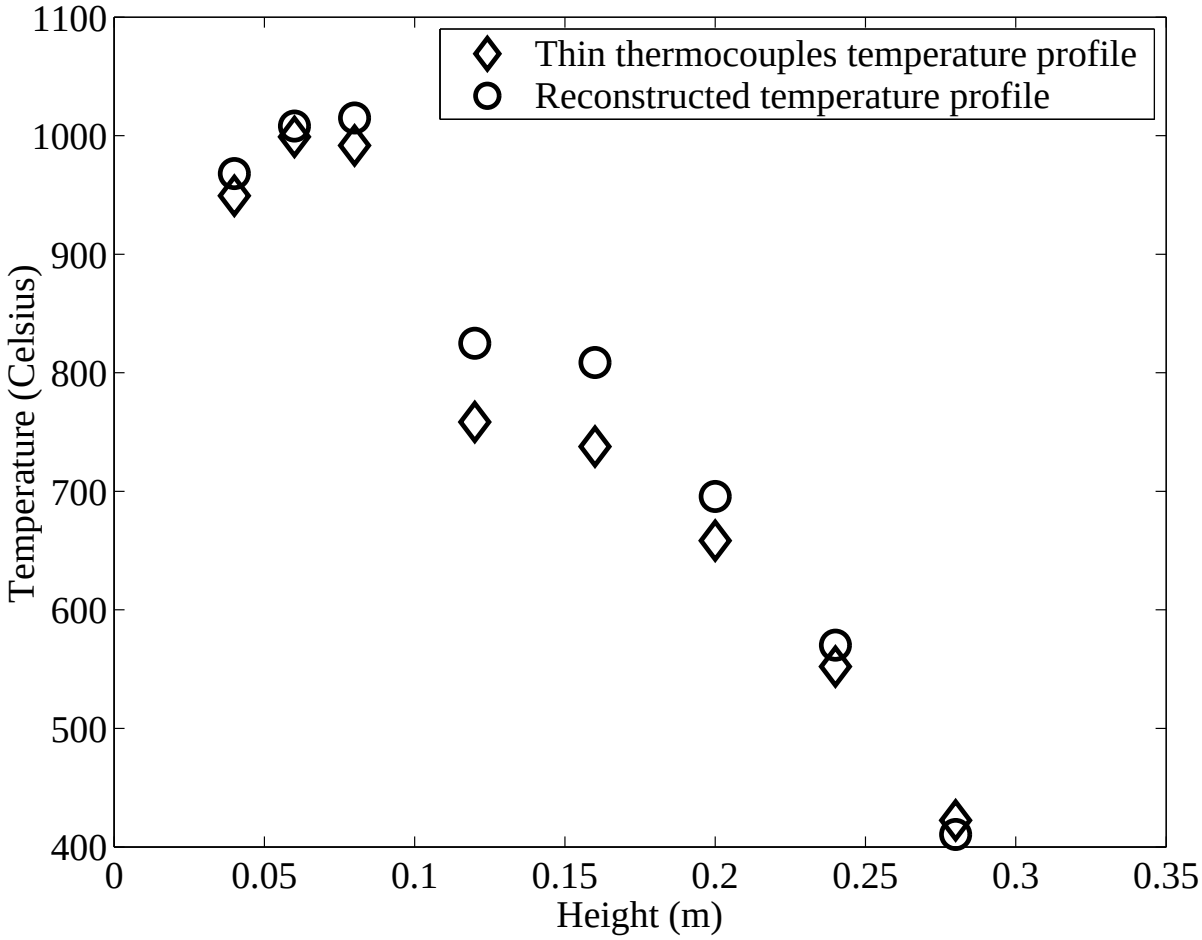

Figure 4: Mean temperature profiles along the fire-plume axis before and after numerical compensation.

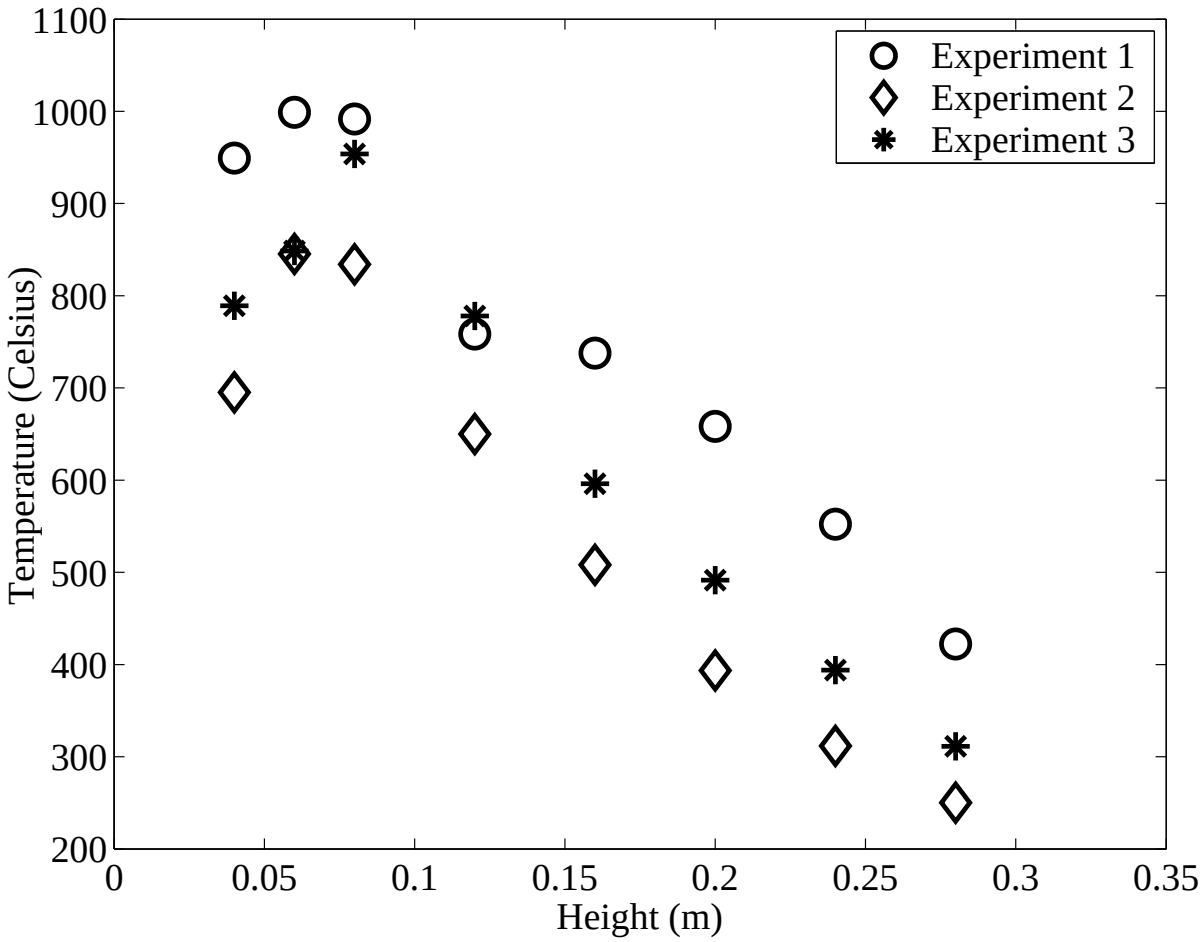

Figure 5: Mean temperature profiles along the fire-plume axis for three experiments.

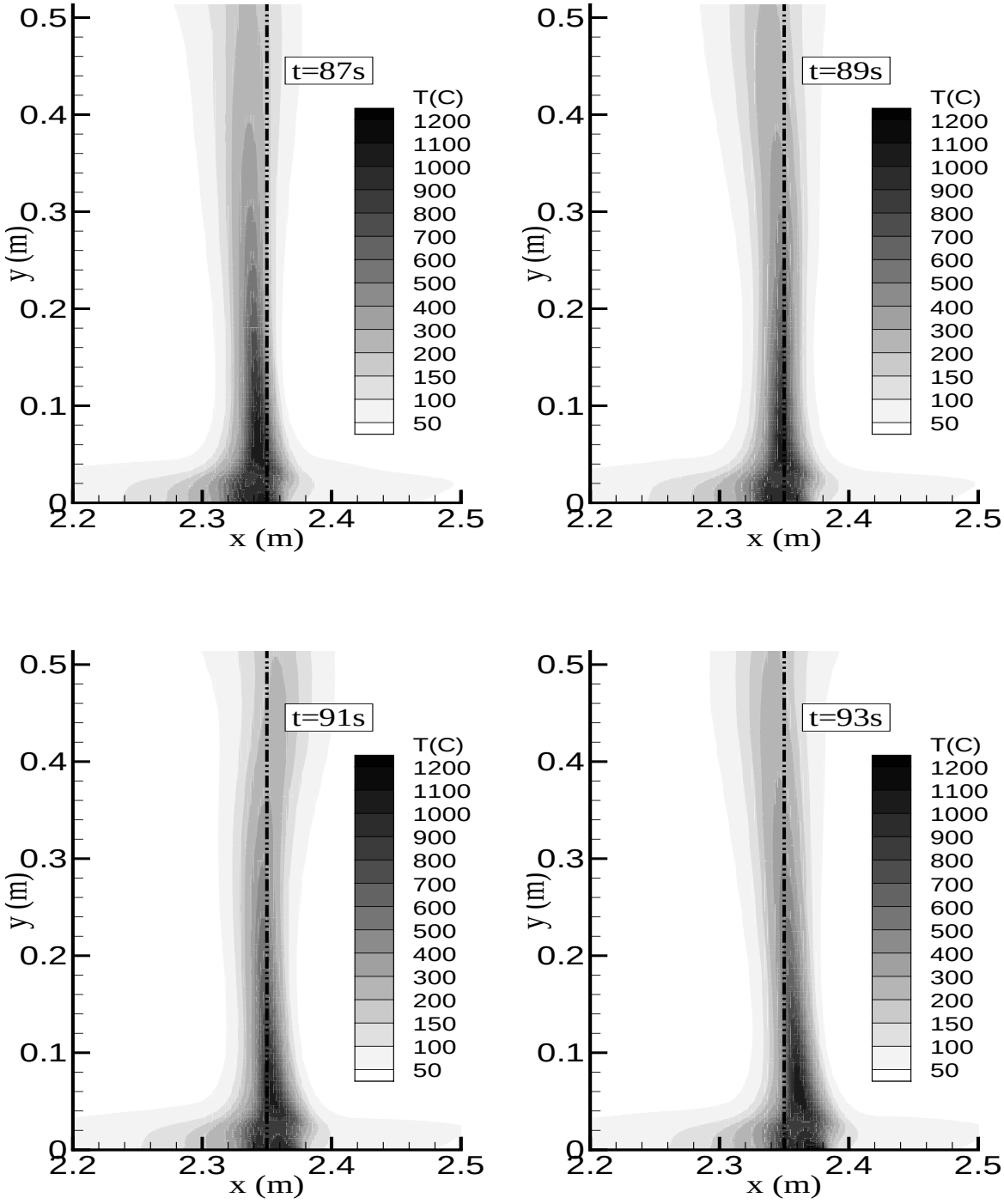

Figure 6: Predicted gas temperature at 90, 94, 98, and 102 seconds when the fire plume comes through the thermocouple tree. The dotted line shows the virtual position of the thermocouple tree.

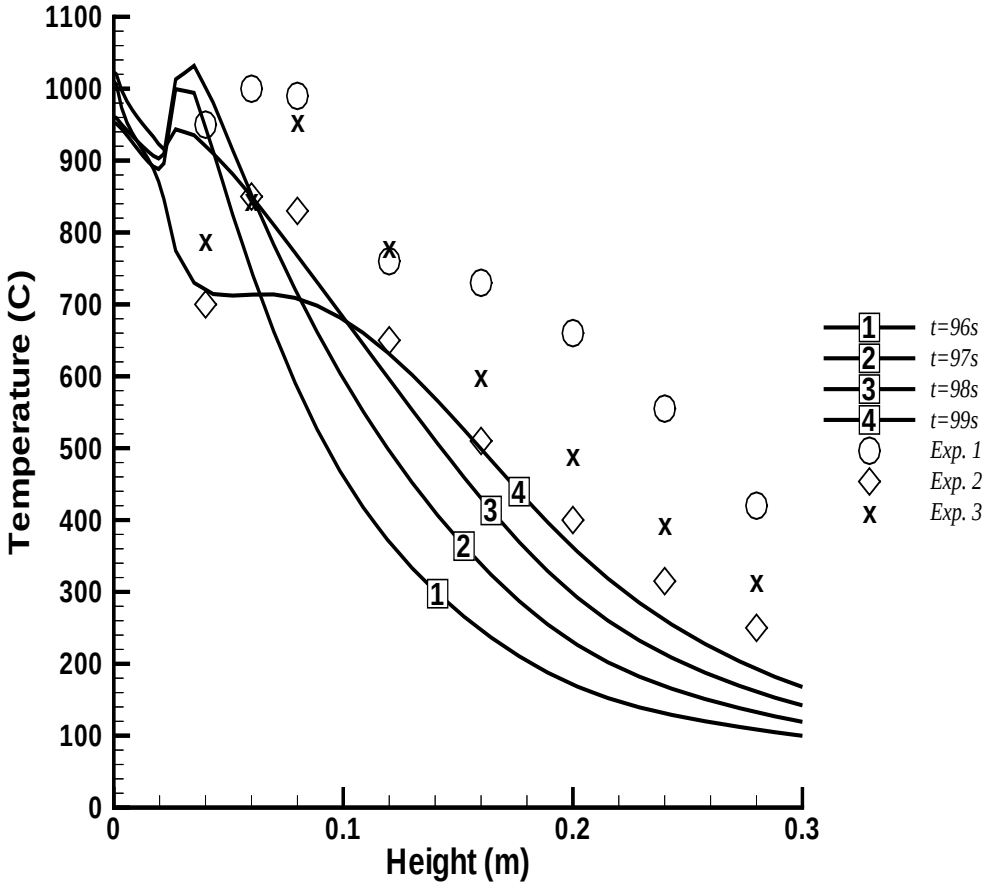

Figure 7: Simulated and experimental temperature profiles along the fire-plume axis.

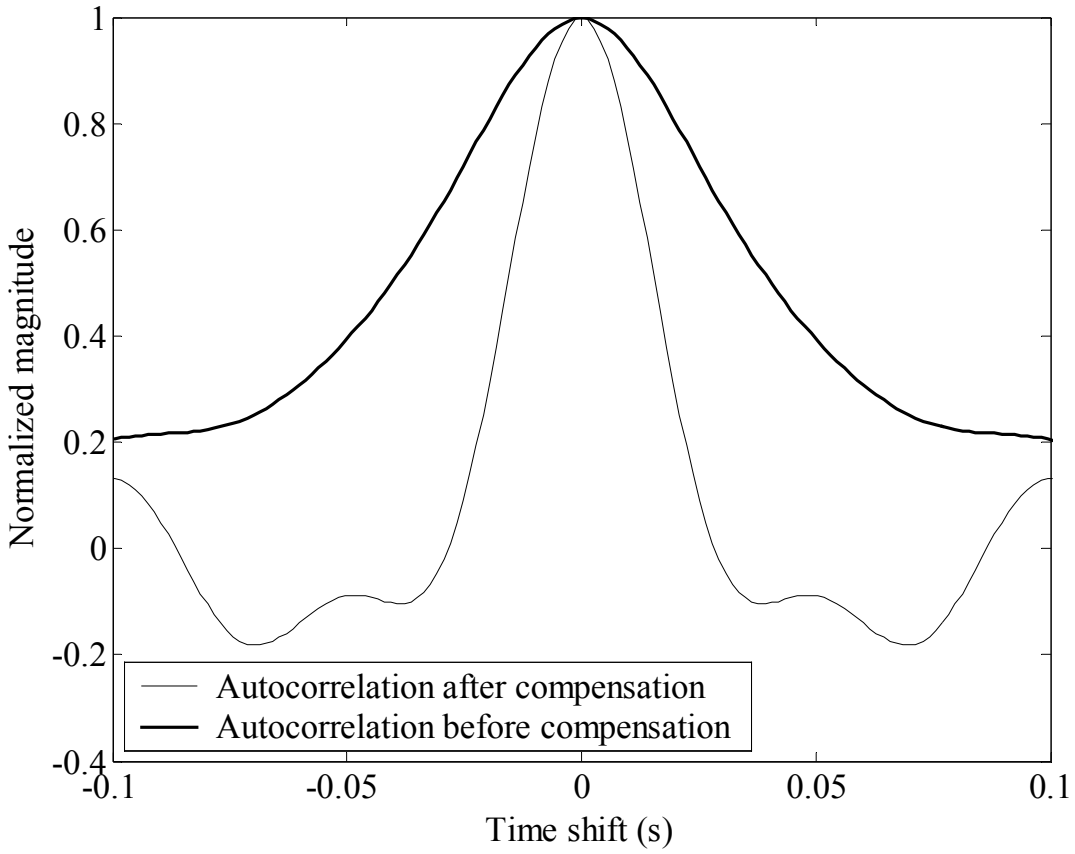

Figure 8: Auto-correlation function before and after numerical compensation for the thin thermocouple of probe 5.

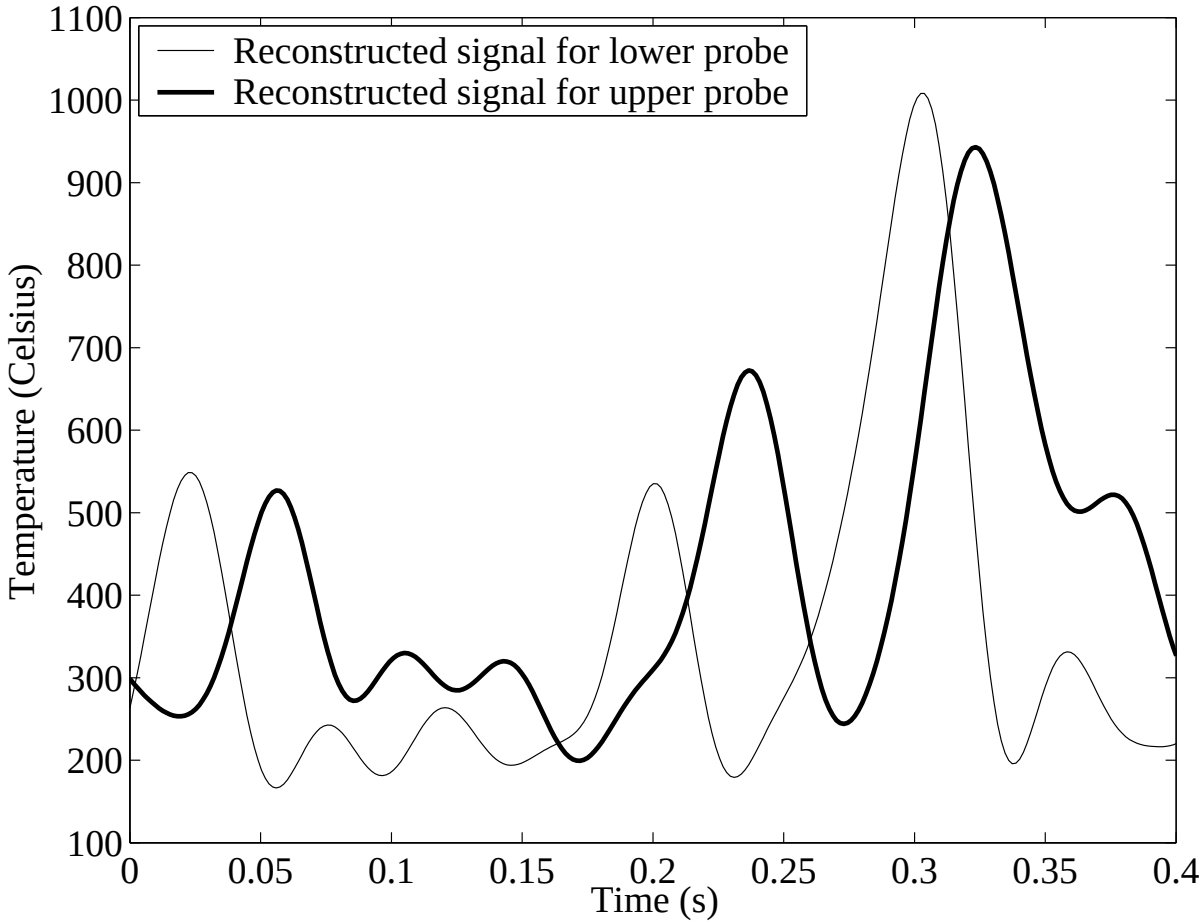

Figure 9: Compensated temperature for the thin thermocouples of two probes 4 cm apart.

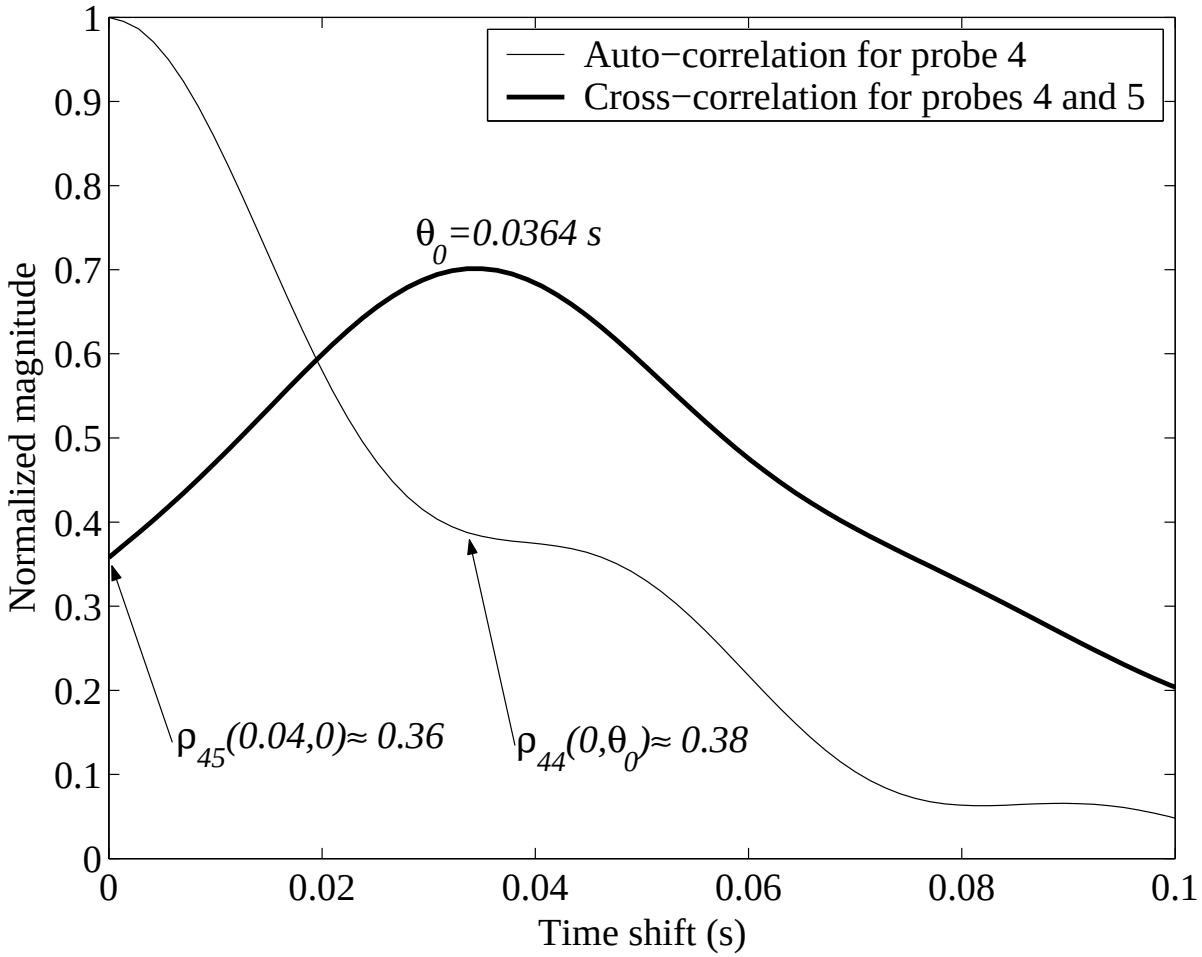

Figure 10: Evaluation of the frozen turbulence hypothesis.

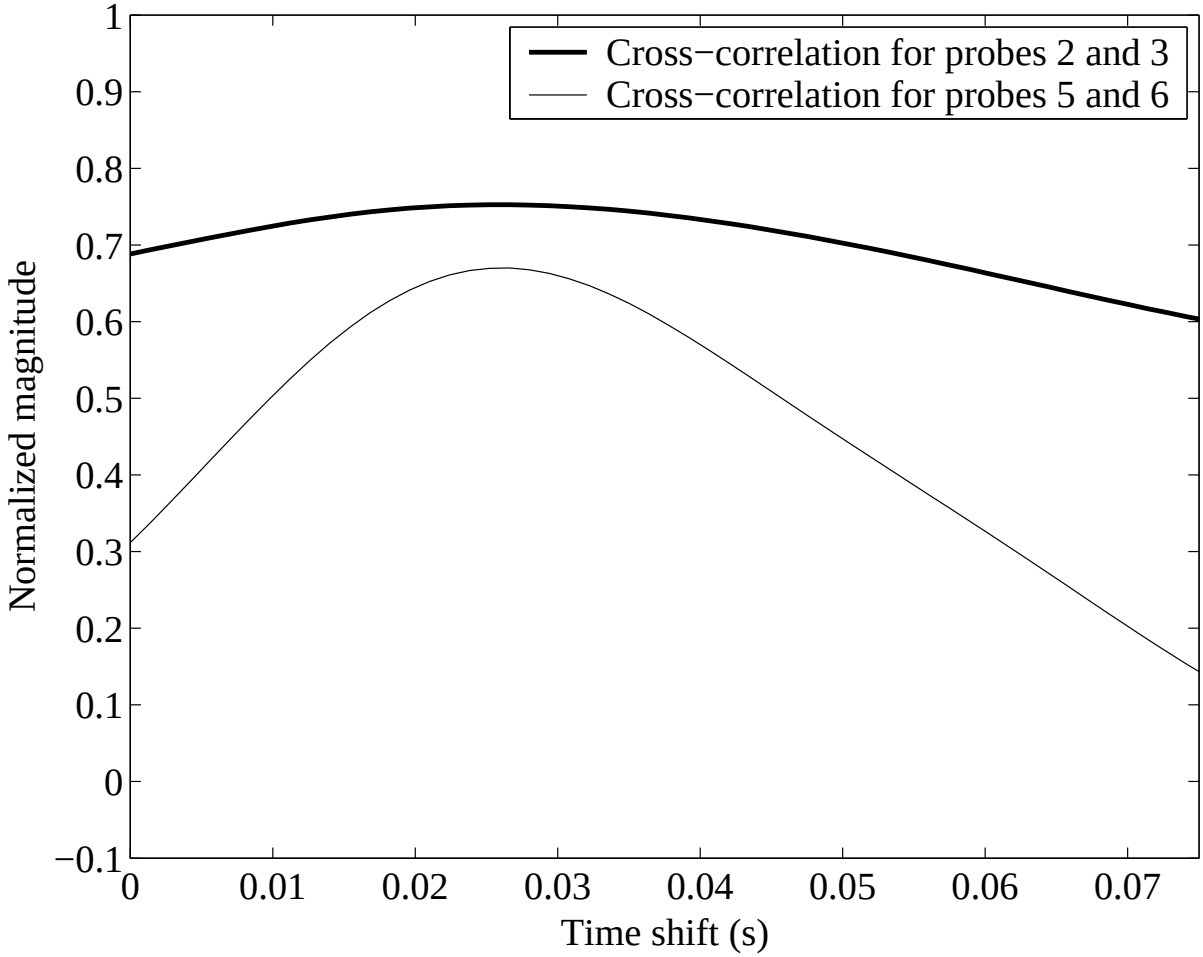

Figure 11: Cross-correlation coefficients of reconstructed temperature at different heights along the fire-plume axis.

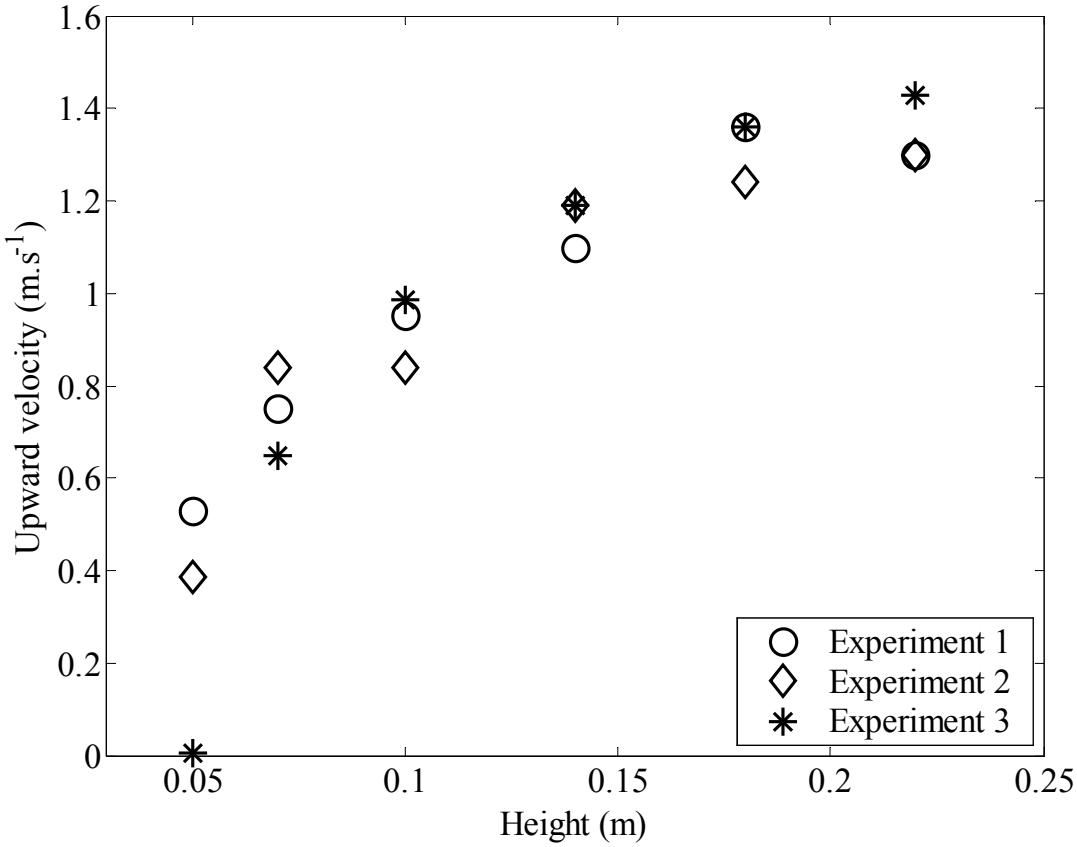

Figure 12: Mean gas velocity profiles along the fire-plume axis.

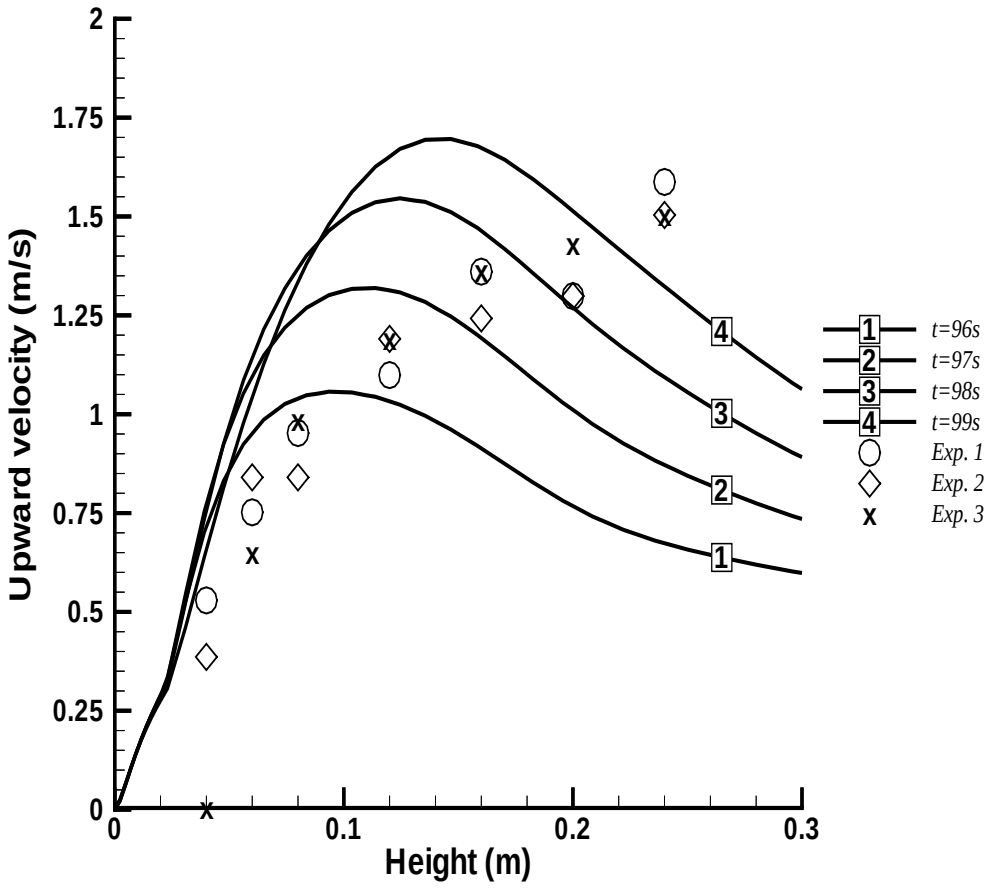

Figure 13: Simulated and experimental gas velocity profiles along the fire-plume axis.